Simulation and structural analysis for the boom of the rocket launcher

I Osama[1], A R Gomaa[2] and A Elsabbagh[1]

[1]Design and Production Engineering Department, Faculty of Engineering, Ain Shams University, 11535, Egypt.
[2] Egyptian Armed Forces.
E-mail: islamosama463@gmail.com

Abstract. The structural design of rocket launcher booms plays a pivotal role in aerospace engineering, requiring a meticulous balance between strength, weight, and durability. This study focuses on the design of rocket launcher booms by analyzing different cross-sectional geometries, including Rectangular Hollow Sections (RHS), I-beams, and their tapered variations. Finite Element Analysis (FEA) was utilized to simulate and assess the performance of each cross-sectional design. Experimental validation involved testing four distinct beam types to measure stress and deformation. Results revealed strong agreement between experimental data and simulation outcomes. Tapered I-beams demonstrated superior performance among the designs, offering low weight, high strength, and minimal deflection, outperforming traditional RHS and standard I-beams. The study's primary objective was to identify the most efficient configuration that minimizes weight while maximizing strength and reducing deformation under both static and dynamic loads. The exceptional performance of tapered I-beams highlights their suitability as the best choice for advanced rocket launcher systems. This research contributes to developing more efficient and reliable launcher booms, paving the way for advancements in aerospace technology and providing critical insights for future design to enhance performance, efficiency, and safety in aerospace applications.

1. Introduction

The design and analysis of rocket launcher booms are essential in aerospace and defense engineering. These structures must endure significant static and dynamic loads while maintaining a lightweight profile to improve mobility and overall efficiency. Traditional approaches typically utilize materials such as steel and aluminum in basic geometric configurations, including rectangular hollow sections (RHS) and I-beams. However, such conventional designs often lead to heavier structures, thereby restricting operational range and payload capacity, as shown in Figure 1.

Numerous studies have been conducted to evaluate and enhance the performance of these structures. Dragoljub Vujic et al. [1] Modeled a rocket launcher system using a combination of solid bodies and deformable elements with damped elastic support. By solving nonlinear differential equations, their study provided significant insights into the design and modification of launcher systems. Serdar Sert and Yigit Tascioglu [2] Developed a dynamic model for a Multiple Rocket Launcher System (MLRS) featuring

electromechanical actuators. They evaluated four different friction models, achieving simulation results with an accuracy of less than 5% error compared to real MLRS test data.

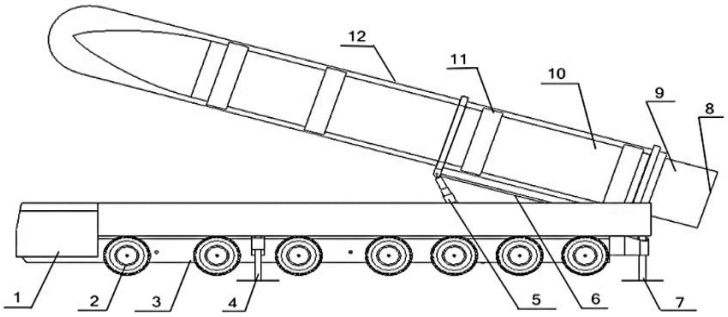

Figure 1. Composition of a Vehicle-Mounted Missile Weapon
1: Front; 2: Wheel; 3: Chassis; 4: Front Levelling Jacks; 5: Erecting Cylinder; 6: Erecting Arm; 7: Rear Levelling Jacks; 8: Adaptive Base; 9: Low Pressure Chamber; 10: Missile; 11: Adapter; 12: Launcher

C. Işık et al. [3] Introduced a flexible multibody model for a missile launcher system, optimizing it by removing insignificant vibration modes and incorporating joint flexibility through spring-damper elements. Li Xue-ping et al. [4] Applied ANSYS to demonstrate the efficacy of topology optimization for improving the design of the winch mounting bracket in an ROV simulator. Deng Biao et al. [5] Performed a finite element analysis (FEA) of a rocket launcher using ANSYS, highlighting the feasibility and cost-effectiveness of this approach while providing valuable insights for improving strength and enabling future equipment upgrades. E.V. Morozov et al. [6] Investigated composite lattice anisogrid shells increasingly used in aerospace applications. They developed an advanced finite-element model generation procedure for buckling analysis of lattice shells, revealing that improving buckling resistance through increased rib stiffness or additional hoop ribs could achieve up to 22% mass savings compared to non-optimized designs. Henry Panganiban et al. [7] Optimized a long-range aerial lift truck's boom using ANSYS Workbench and HyperWorks. Their work refined cross-sectional dimensions of wall thickness and achieved a 250-kg (2.2%) weight reduction, a 33% increase in stiffness, and a 59% improvement in torsional frequency. Erasmo Carrera and Enrico Zappino [8] Proposed advanced structural models with variable one, two, and three-dimensional kinematics for analyzing the free vibration of reinforced aircraft shell structures. Unlike classical theories, their models utilized Lagrange polynomials for displacement fields and FEM for numerical solutions, offering more accurate and computationally efficient results.

Xinlin Wei et al. [9] Developed lumped parameter and dynamic models in ADAMS to study coupling effects between a missile system and its launching site. Co-simulation with MATLAB/Simulink highlighted that vertical slip was more significant than other directions, identifying surface layer thickness as the most critical factor for stability. Experimental data for plume force and motor thrust validated their model, accurately representing the launcher system's behavior. Jia Yao et al. [10] Performed nonlinear finite element analysis (FEA) on an all-terrain crane's telescopic boom to investigate failure mechanisms. Using simplified and detailed models, they analyzed geometric and contact nonlinearity, determining that while overall strength met the criteria, stress wrinkles in the 5th boom section indicated elastic buckling as the primary cause of failure. I. Adamiec-Wojcik et al. [11] Developed a nonlinear static model for a 700mT lattice-boom crane using the rigid finite element method. Their software accounts for the flexibility of the rope system and provides precise calculations of forces, stresses, and displacements. The results were validated against the ROBOT software, demonstrating high accuracy. Ana Pavlovic et al. [12] Analyzed telescopic booms' structural resistance and stability using ANSYS. Their findings confirmed that stresses remained within elastic limits, with critical loads and buckling modes exceeding extreme

conditions, ensuring stability. The use of FEM simulations minimized the need for extensive physical experiments and facilitated design optimization. Cristiano Fragassa et al. [13] Examined the response of a large telescopic boom to intense static and dynamic loads. Combining traditional design approaches with specific tests ensured safety and validated design assumptions. The study also measured deformations to investigate local instability phenomena that theoretical models often fail to predict. Samet Dönerkaya et al. [14] designed and developed a prototype for a next-generation ingot crane tailored to the iron and steel industry. Their work utilized both analytical methods and Finite Element Analysis (FEA) to determine maximum stress and deflection values, focusing on Von Mises stress in critical areas. This study investigates advanced design methodologies, with a focus on Finite Element Analysis (FEA), to determine the cross-sectional geometries for lightweight and structurally rocket launcher booms.

2. Methodology

As with other applications, measuring deformations and stresses in the boom of a rocket launcher involves using strain gauges to monitor critical stress points. This data is crucial for validating the design and ensuring the boom's reliability during key operations such as launch and transportation. Potential enhancements may focus on the selection of the material, cross-section, and overall boom design to effectively manage static stresses, thereby improving performance and safety.

2.1. Case study

This study begins with an examination of a specific rocket launcher boom, as shown in Figure 2. Four configurations were tested to see which one was the most stress-resistant and lightest, providing technical insights into their safety and stability.

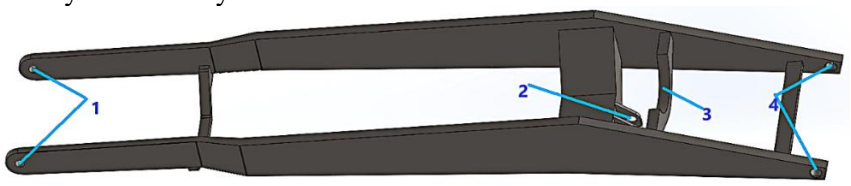

Figure 2. Rocket Launcher Boom Case Study
1-Front Load, 2-Lifting Point, 3-Rear Load, 4-Rotation Axis

Key aspects of mechanical systems are also addressed to enhance overall performance;

1) Length (L): 1500 mm (1000 mm straight segment and 500 mm segment at a 15-degree angle).
2) Width (B): 100 mm (consistent across all sections).
3) Nominal Load (F): 400 kg (approximately 3924 N, with g = 9.81 m/s²).
4) Material: St (37) and its properties are listed in Table 1.

Table 1. Material Data

Material	Young's Modulus (E)	Poisson's Ratio (ν)	Yield Strength (σy)	Density (ρ)
St 37	210 GPa	0.3	250 Mpa	7850 kg/m³

This study is developed through the following phases:

1) **Conceptual Design**: The initial phase involves defining the geometry, loading conditions, and constraints for a case study.

2) **Simplification**: Theoretical models are simplified to estimate stresses and deformations under various load conditions.
3) **Modeling**: Detailed 3D CAD designs are created for the prototype and testing equipment.
4) **Numerical Analysis**: Finite Element Analysis (FEA) is applied to explore potential unexpected phenomena, evaluating stresses and strains to assess the system's usability, resistance, and stability under various loading conditions.
5) **Integration of Evidence**: Experimental data is combined with FEM analysis to enhance the understanding of the structure's response to working loads. This mechanism includes a beam with three supports, one for a concentrated load and two fixed supports, as shown in Figure 3.

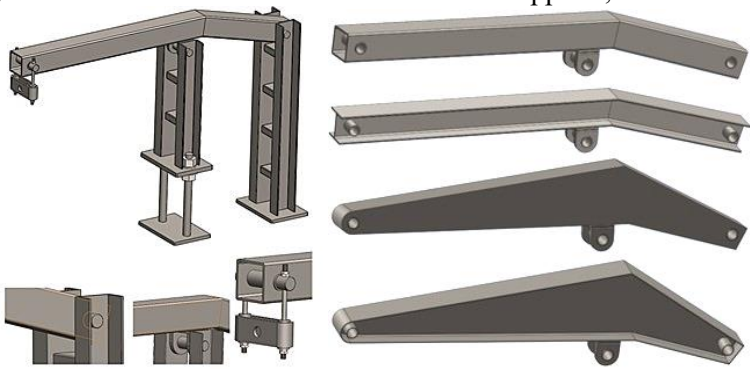

Figure 3. Four Configurations with Testing System

2.2. Analytical model

Theoretical analysis of forces and moments acting on the system was performed using a simplified model for four configurations, as shown in Figure 3.This approach reflects realistic usage conditions, incorporating applied loads and constraints. The investigation focuses on the most critical stressed zones, ensuring the analysis addresses the key areas affecting the system's performance and stability.

The simplest model for the system is represented by a beam fixed at one end with a double hinge and free at the other, as shown in (Figure 4(a)). This model simplifies the structure into a straight prismatic beam with two perpendicular flat bases near the load application, where mass forces are negligible compared to external loads. The beam is largely unconstrained, resembling Lamé's problem. According to De Saint Venant's Principle [15], replacing a system of forces with a statically equivalent one (with the same magnitude and resultant torque) does not affect the stress distribution at points far from the load application. This principle allows the system to be treated as a slender beam with a predominant length, experiencing small displacements and loads applied at its ends. While this simplification omits localized effects and abrupt profile changes, it enables quick and reliable calculations to identify critical areas. Further simplification is achieved by applying De Saint Venant's theory to thin-walled beams with hollow square cross-sections and a wall thickness of 6 mm, which resemble the C-beams used in the construction of the boom's trunks. The theoretical analysis, based on De Saint Venant's theory for thin beams, focused on calculating the following parameters: Moment of inertia (neutral axis) for four sections, Reaction forces, Shear and bending moment diagrams, Normal stress, Shear stresses (using Jourawski's model, applicable to thin closed sections), and Equivalent stresses (based on the Von Mises criterion). The stresses were primarily influenced by bending moments. The bending moment exhibited a linear increase, depending on the variability of the cross-sections, with a nearly constant maximum value occurring in the central zone, as shown in (Figure 4(b)). Given the negligible shear stress, as shown in (Figure 4(c)). The contribution of shear was disregarded. Therefore, the geometry became a critical factor in identifying the most stressed sections[16] . A beam is subjected to a force applied at point C with two supports at points

A and B. The distances between the points are AB = 500 mm and BC = 1000 mm. Using the equilibrium equations [17], The moment around B is:

$$M_B = -3924000\ N.mm$$

The stress resulting from a force of F = 3924 N was calculated to be 50.51 MPa, which is well below the yield strength of St 37 (~250 MPa). This analysis demonstrates that, despite the limitations of simplified models, the rocket launcher boom is designed to withstand significantly higher loads.

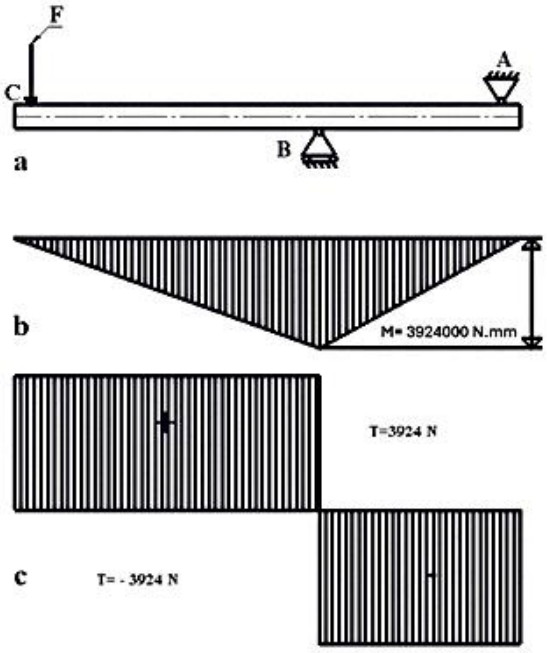

Figure 4. Schematic Loads and Constraints, Bending Moment (M), and Shear Force (T)

3. Numerical Simulations

Numerical simulations leverage computational models to predict structural behavior under various conditions with different erecting angels, sequentially 30°, 45°, and 60°, as shown in Figure 5 .

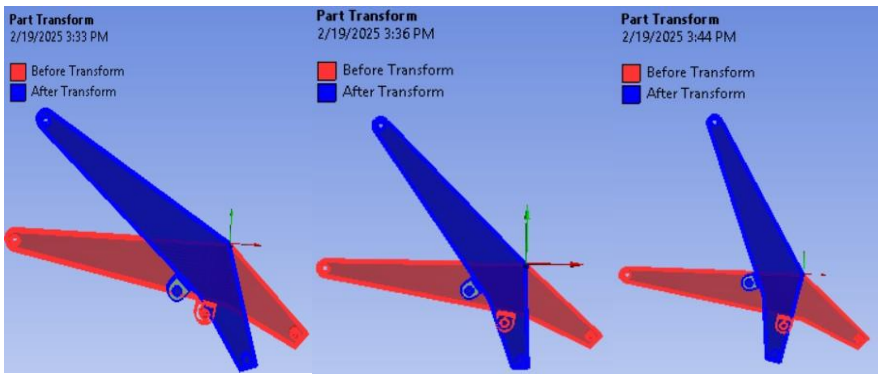

Figure 5. Model Orientation

3.1. Model meshing

The beam is modeled using a finite element mesh with 3D elements, such as solid or beam elements, depending on the geometry and accuracy needs. The mesh is refined near the supports and force

application point to accurately capture stress concentrations and displacement gradients. Building on initial simplifications, progressively more complex models were developed to simulate geometries and conditions closely resembling the real structure. Finite element simulations were performed using ANSYS WB 20R1. The FEM was discretized with 10-node tetrahedral elements, chosen based on the model's size to ensure accuracy while keeping the number of nodes manageable, as shown in Figure 6. This approach provided quick and precise numerical solution [18, 19]. To improve computational efficiency and accuracy, the element size was refined in critical areas, resulting in a final discretization of over 50,000 elements and 116,000 nodes for rectangular hollow cross-section, over 53,000 elements and 120,000 nodes for tapered hollow cross-section, over 45,000 elements and 105,000 nodes for I-beam cross-section and over 40,000 elements and 97,000 nodes for tapered I-beam cross-section.

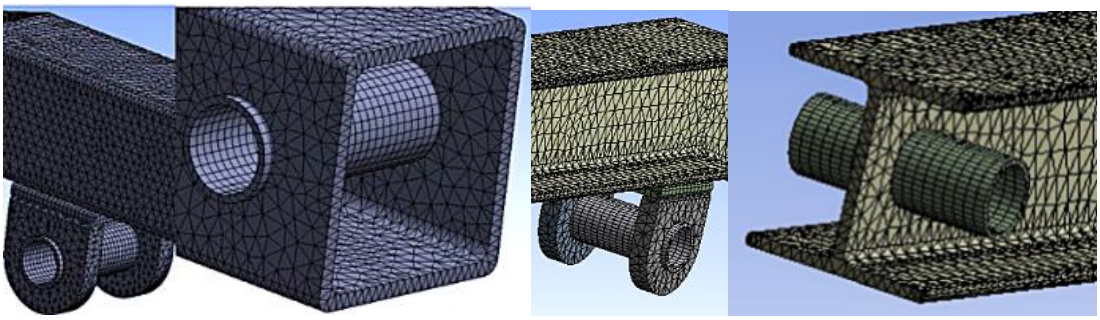

Figure 6. Mesh for All Configurations.

3.2. grid sensitivity

A grid sensitivity analysis was performed by discretizing the beam model with progressively smaller elements. Nine grids were evaluated, with element sizes ranging from 30 mm to 3 mm, to observe how maximum stress values changed with an increasing number of elements. As shown in Figure 7, significant changes in maximum stress occurred with coarse grids. For mid-sized grids, the variation in maximum stress decreased, and for the two finest grids (6 mm and 3 mm element sizes), the maximum stress values were nearly identical. This suggests that further reduction in element size does not affect the stress values, confirming a grid-independent solution at a 6 mm element size.

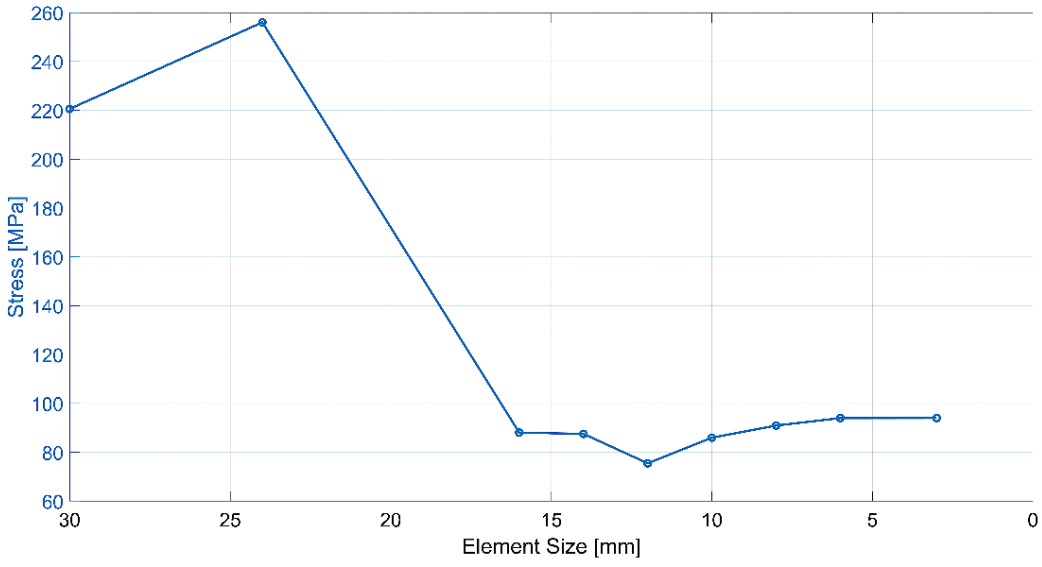

Figure 7. Maximum Stress Variation with Element Size

3.3. Boundary conditions

Boundary conditions were applied at the two support points, incorporating frictional constraints that permit limited sliding while preventing rigid-body motion. This approach simulates realistic conditions where resistance exists but does not result in perfect fixation. Contact elements were used to model the interaction between the beam and its supports, with a friction coefficient defining the resistance to movement. The finite element mesh was designed to respect the beam's symmetry, reducing computational effort while maintaining accuracy.

Gravitational forces were also considered, acting uniformly along the beam to account for its weight. Fixed Support is pivotal in ensuring the stability and integrity of the structure, preventing any unintended movement or displacement. The system is subject to standard Earth gravity, with a gravitational acceleration of 9806.6 mm/s² and a vertical force on a mechanical system. The force with a magnitude of 3924 N. To verify the finite element (FE) dimensions, several simulations were conducted using different meshes, and the results were compared, considering computational time. A grid-independent solution was achieved with a 6 mm element size in the critical area near the junction. A moderately sparse mesh with a 10 mm element size was applied to the remaining parts of the boom. This approach ensures a balance between accuracy and computational efficiency for the overall model.

3.4. Simplified model

To expedite an initial approximate numerical simulation, a simplified "single body" model was developed. This model assumes that all assembly components comprising over forty parts are welded into a single piece made from the same material (St 37)[20]. These simplifications were introduced to temporarily bypass the complexities of modeling contact interactions between surfaces, which would otherwise require managing over 100 contacts [21]. The model is fixed to the system using two pins, with a load applied at the tip of the beam for four configurations. This homogeneous model, characterized by its low computational time (requiring only 6 to 8 hours), facilitated a broad range of simulations and numerical result comparisons.

4. FEM Simulation Results

As expected, the lowest values of stress appeared at points (a) (load application), and (c) (rotation axis), Figure 8 Shows the max stress value at section (b) (erecting arm) for configurations as the area of stress concentration and the deformation distribution.

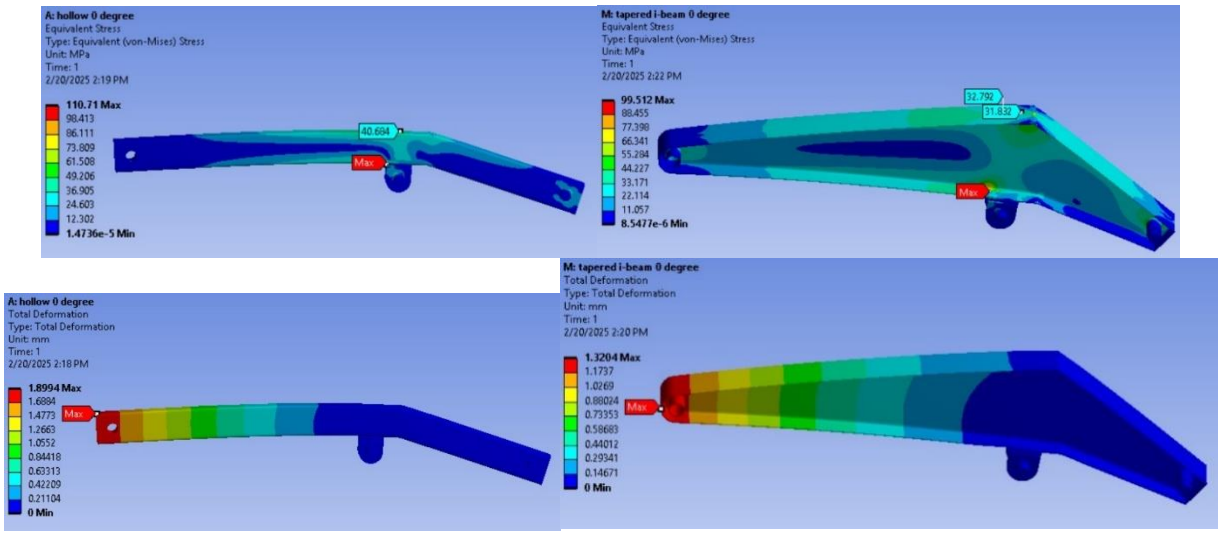

Figure 8. Stress and Deformation Distribution for Configurations

4.1. Comparison Between Experimental and FEM Simulation Results

The position of the strain gauge is checked by a probe used in ANSYS simulation so results from simulations can be compared against experimental ones, as shown in Figure 9.The behavior of the structure is examined at different loads. It can be noticed that the maximum percentage difference is equal to 15% at the maximum load between the simulation and the experimental. Differences between simulation results and experimental measurements can arise due to various factors [22]. Simulations rely on mathematical models that make assumptions about the system. Material properties in experiments reflect actual conditions, whereas simulations often use idealized or averaged values, leading to discrepancies.

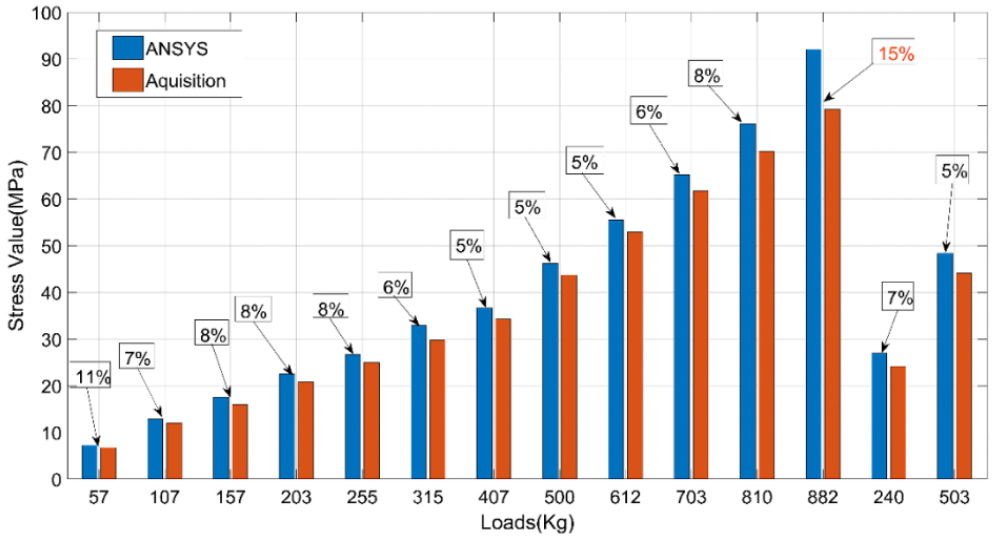

Figure 9. Comparison Between ANSYS and Acquisition Data for 1st Strain Gauge of Tapered I-Beam Configuration

Environmental factors such as temperature, humidity, and vibrations can influence experimental results, while measurement errors may arise from instrument precision limitations or human factors. Scale effects can also contribute to variations. Conversely, the maximum stress value can't be the only factor determining the best configuration. The same material, St 37, is used for all models, which means the same strength value of 250 Mpa. As the main difference is model geometry, which affects model weight and stress, the combination of these factors will be the key factor when selecting the most efficient model. This is weight to stress ratio, the differences between weight-to-stress and strength ratios are shown in
Since the stress value for a model has a direct effect on the safety factor under certain load conditions[23], The safety factor for each configuration, which should be more than 1.4, is calculated according to this equation:

$$\boldsymbol{SF = \frac{Ultimate\ Strength}{Allowable\ Strength}} \qquad (1)$$

Table ***3*** presented simulation and experimental results at a nominal load of 400 kg at a location of 1st strain gauge. It can be concluded that all configurations are safe under the same loading condition with a minimal safety factor of 3.77 more than 1.4. In addition, there is another piece of evidence for the good accuracy of simulation results against experimental measurements with a maximum deviation of 12%. So, the weight-to-stress ratio is considered a judging factor in the present study's selection of the most efficient configuration.
Table *2*.

Since the stress value for a model has a direct effect on the safety factor under certain load conditions[23], The safety factor for each configuration, which should be more than 1.4, is calculated according to this equation:

$$\boldsymbol{SF = \frac{Ultimate\ Strength}{Allowable\ Strength}} \qquad (1)$$

Table ***3*** presented simulation and experimental results at a nominal load of 400 kg at a location of 1st strain gauge. It can be concluded that all configurations are safe under the same loading condition with a minimal safety factor of 3.77 more than 1.4. In addition, there is another piece of evidence for the good accuracy of simulation results against experimental measurements with a maximum deviation of 12%. So, the weight-to-stress ratio is considered a judging factor in the present study's selection of the most efficient configuration.

Table 2. Difference Between Weight-to-Stress and Strength Ratios

Ratio type	Weight-to-Stress Ratio	Weight-to-Strength Ratio
Definition	Compares the weight of a structure to the stress it experiences under specific loading conditions.	Compares the weight of a structure or material to its maximum strength.
Formula	$\frac{\text{Weight of the Structure}}{\text{Stress under Applied Load}}$	$\frac{\text{Weight of the Structure}}{\text{material strength}}$

Key Points	Stress is dependent on the applied forces and geometry of the structure.	Strength refers to the material's ultimate or yield strength.
Main Difference	Stress is an actual response to loading and depends on the applied forces, geometry, and boundary conditions.	Strength is an inherent property of the material, defining its maximum capacity to resist stress before failure.

Table 3. Safety Factor Calculations

Configuration Type	Simulation Stress (Mpa)	Experimental Stress (Mpa)	Simulation Safety factors	Experimental Safety factors	Deviation
R-Hollow	66.38	63.63	3.77	3.92	3%
T-Hollow	27.26	25.62	9.17	9.75	6%
I-Beam	55.11	48.3	4.54	5.18	12%
T-I-Beam	35.15	33.43	7.11	7.48	5%

Error! Not a valid bookmark self-reference. Represents the weight-to-stress ratio and the safety factor at a nominal load (400 kg) for all beam configurations according to simulation results. Tapered I-Beam is minimizing weight while maintaining structural integrity is crucial as shown in **Error! Not a valid bookmark self-reference.**, it offers the lowest weight (14.94 kg) and a good factor of safety (2.51). Its weight-to-stress ratio (0.172) is lower than the other sections, so it performs effectively under load conditions. In contrast, while the Tapered Rectangular Hollow Section provides a higher factor of safety and better stress distribution, it does not offer weight reduction as the Tapered I-Beam, making the latter more efficient for weight-sensitive applications.

Table 5 presents a stress and deformation comparison with all erecting angels. The highest stress and deformation values were observed at a zero-degree angle, as this position corresponds to the maximum moment arm for the applied load. This results in greater bending effects and stress concentrations compared to other angles. Consequently, the structural response is most critical at this orientation, requiring careful consideration in design and analysis.

Table 4. Weight-to-Stress Ratio Values for All Configurations

Configuration Type	Weight (kg)	Max-Stress (Mpa)	Safety Factor	Weight-to-Stress Ratio
R-Hollow	29.2	110.71	2.26	0.311
T-Hollow	23.35	86.06	2.9	0.345
I-Beam	23.33	113.59	2.2	0.226
T-I-Beam	14.94	99.51	2.51	0.172

Table 5. Comparison Between All Configurations

Configuration Type			R-Hollow	T-Hollow	I-Beam	T-I-Beam
0 degree	Stress Value (Mpa)	Max	110.71	86.06	113.59	99.51
		Probe	40.68	22.45	49.94	32.79
	Deformation (mm)		1.89	1.04	2.33	1.32
30 degrees	Stress Value (Mpa)	Max	98.06	69.78	101.24	78.43
		Probe	34.17	18.39	44.89	25.45
	Deformation (mm)		1.7	0.86	1.99	1.05
45 degrees	Stress Value (Mpa)	Max	81.33	51.62	84.37	59.37
		Probe	27.39	13.44	35.57	18.97
	Deformation (mm)		1.32	0.68	1.62	0.81
60 degrees	Stress Value (Mpa)	Max	60.88	28.56	61.75	36.23
		Probe	18.84	9.13	22.59	11.89
	Deformation (mm)		0.93	0.44	1.13	0.51

Figure 10 Shows weight-to-stress ratio according to the experimental results of 1st strain gauge for all configurations with all loads. Obeying the same conclusion from simulation results, the tapered I beam is the best configuration according to the weight-to-stress ratio.

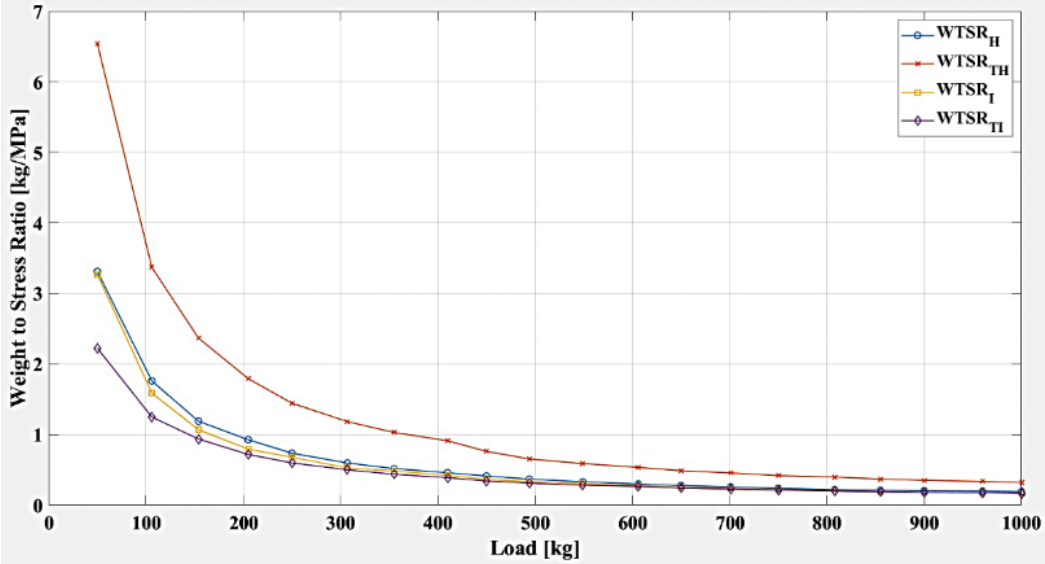

Figure 10. Weight-to-Stress Ratio for 1st Strain Gauge (All Configurations)

5. Conclusions

Structural design of rocket launcher booms is conducted, and a combination of theoretical analysis, FEM simulations, and experiments was presented to configure which structure configuration is more suitable to achieve a minimum weight-to-stress ratio. Four types of configurations are selected for this comparison (I-beam, hollow, tapered hollow, and tapered I-beam).

By integrating theoretical predictions, simulations, and experimental results, the model under investigation was refined to enhance the design and achieve the desired safety factor with minimum weight.

Analysis and comparison between results from both experimental and FEM simulations showed:

- The maximum stress difference was 15% at maximum load, which verifies a 1.4 safety factor. while the average difference was 8% with different loads.
- This accuracy percentage provides good evidence that FEM is an accountable tool that can be relied on during the conceptual design phase for boom structures.
- Tapered I-beam configuration can satisfy the lowest weight-to-stress ratio.
- Tapered I-beam configuration provides a weight saving of 50 % without losing structural stability.

In future work, it is recommended to use more real assumptions during modeling to improve FEM accuracy. Vibration analysis with more cross-sectional configurations with different materials should be taken into consideration, seeking a more stable launcher boom.

References

[1] Djurkovic V, Milenkovic N and Trajkovic S 2021 Dynamic analysis of rockets launcher *Tehnički vjesnik* 28 530-9

[2] Sert S and Tascioglu Y 2015 Dynamic Modeling of a Multiple Launch Rocket System. In: *Proceedings of the World Congress on Engineering*

[3] Işık Ç, Ider S and Acar B 2014 Modeling and verification of a missile launcher system *Proceedings of the Institution of Mechanical Engineers, Part K: Journal of Multi-Body Dynamics* 228 100-7

[4] Li X-p, Zhao L-y and Liu Z-z 2017 Topological optimization of continuum structure based on ANSYS *MATEC Web of Conferences: EDP Sciences* p 07020

[5] Deng B, Guo Y, Zhang A and Tang S-j 2017 Finite element analysis of large rocket launcher 2017 *5th International Conference on Frontiers of Manufacturing Science and Measuring Technology* pp 1132-9
[6] Morozov E, Lopatin A and Nesterov V 2011 Buckling analysis and design of anisogrid composite lattice conical shells *Composite Structures* 93 3150-62
[7] Panganiban H, Ahn I-G and Chung T-J 2012 Multi-phase Design Optimization of a Long Range Aerial Lift Boom Structure *World Congress on Engineering* pp 1697-700
[8] Carrera E and Zappino E 2016 Carrera unified formulation for free-vibration analysis of aircraft structures *AIAA Journal* 54 280-92
[9] Wei X, Jiang Y, Zeng W and Pan X 2016 The coupling effects of the missile launcher and the ground in vehicle-mounted missile erecting *Advances in Mechanical Engineering* 8 1687814016656106
[10] Yao J, Qiu X, Zhou Z, Fu Y, Xing F and Zhao E 2015 Buckling failure analysis of all-terrain crane telescopic boom section *Engineering Failure Analysis* 57 105-17
[11] Adamiec-Wójcik I, Wojciech S and Metelski M 2018 Application of the rigid finite element method to static analysis of lattice-boom cranes *International Journal of Applied Mechanics Engineering* 23 803-11
[12] Pavlovic A, Fragassa C and Minak G 2017 Buckling analysis of telescopic boom: theoretical and numerical verification of sliding pads *Tehnički vjesnik* 24 729-35
[13] Fragassa C, Minak G and Pavlovic A 2020 Measuring deformations in the telescopic boom under static and dynamic load conditions *Facta Universitatis, Series: Mechanical Engineering* 18 315-28
[14] Dönerkaya S, Kök K, Eroğlu C and Zeyrek K 2023 New Generation Ingot Crane Design, Finite Element Analysis (FEA) and Prototype Manufacturing *The European Journal of Research Development* 3 280-97
[15] Pian T H and Tong P 1969 Basis of finite element methods for solid continua *International Journal for Numerical Methods in Engineering* 1 3-28
[16] Craig Jr R R and Taleff E M 2020 *Mechanics of materials: John Wiley & Sons*
[17] Samuelson P A 1941 The stability of equilibrium *comparative statics and dynamics Econometrica: Journal of the Econometric Society* 97-120
[18] Dhatt G, Lefrançois E and Touzot G 2012 Finite element method *John Wiley & Sons*
[19] Bin Kamarudin M N, Mohamed Ali J S, Aabid A and Ibrahim Y E 2022 Buckling analysis of a thin-walled structure using finite element method and design of experiments *Aerospace* 9-541
[20] Rakin M, Arsić M, Bošnjak S, Gnjatović N and Međo B 2013 Integrity assessment of bucket wheel excavator welded structures by using the single selection method *Tehnicki vjesnik-Technical Gazette* 20 811-6
[21] Ikhenazen G, Saidani M and Chelghoum A 2010 Finite element analysis of linear plates buckling under in-plane patch loading *Journal of constructional steel research* 66 1112-7
[22] Toma M, Guru S K, Wu W, Ali M and Ong C W 2021 Addressing discrepancies between experimental and computational procedures *Biology* 10 536
[23] Zipay J J, Modlin C T and Larsen C E 2016 The ultimate factor of safety for aircraft and spacecraft-its history, applications and misconceptions *57th AIAA/ASCE/AHS/ASC Structures, Structural Dynamics, and Materials Conference* p 1715